Ion States Impact Charge Transport and Dielectric Constant for Poly(ethylene oxide)based Sulfonylimide Lithium Ionomers

Wenwen Mei¹, Deyang Yu², Louis A. Madsen², Robert J. Hickey^{1,3,*}, Ralph H. Colby^{1,3,*}

¹Materials Science and Engineering, The Penn State University, University Park, PA16802, USA

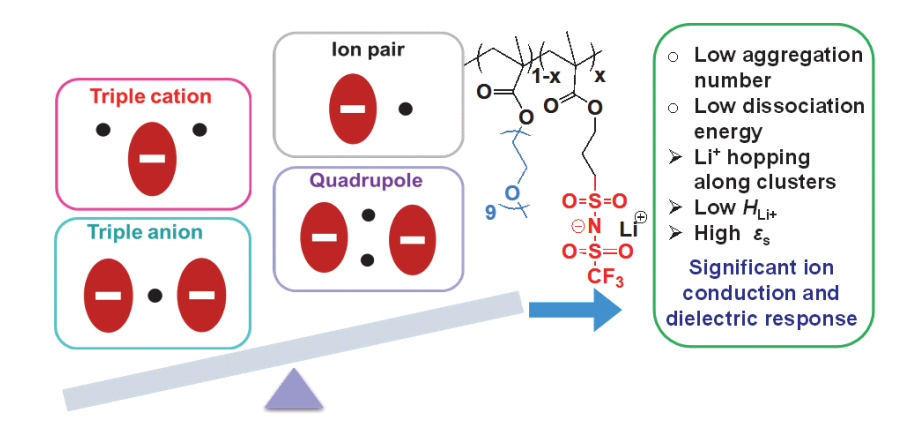
²Department of Chemistry and Macromolecules Innovation Institute, Virginia Tech, Blacksburg,

VA 24061

³Materials Research Institute, The Penn State University, University Park, PA16802, USA

*Corresponding Authors: rjh64@psu.edu and rhc5@psu.edu

TOC



Abstract

Understanding dielectric response and charge transport in ion-containing polymers is essential for the design and implementation of these materials in energy-related applications. Our previous study identified the significant impacts of anion chemical composition on ion conduction for poly(ethylene oxide)-based lithium ionomers with polymer-fixed sulfonylimide (MTLi) and sulfonate counterions (J. *Mater. Chem. C*, 2022, 10, 14569). In this study, we further explore the dielectric response and Li⁺ conduction in the context of different ion states using DFT. The most relevant ion states impacting the dielectric response and Li⁺ conduction are represented with a four-state model. DFT calculation using cluster continuum solvation model captures the local solvation effects of poly(ethylene oxide) and reveals low cluster dissociation energy between neutral and charged states. Low cluster dissociation energy explains the weakly aggregated morphology with low aggregation number based on X-ray scattering pattern and implies that Li⁺ rapidly exchanges between different ion states. Consequently, Li⁺ can hop along aggregates for high ion content MTLi which results in its significant dielectric response, comparable conductivity, and lower Haven ratio despite stronger aggregation than the low ion content counterparts. Different from typical ionomers where raising ion content is detrimental to the ion transport and dielectric response, the understandings based on different ion states for MTLi offer new insights to promote ion conduction and dielectric response for single-ion conducting ionomers.

Introduction

Single-ion conducting ionomers are potential materials for applications such as solid-state electrolytes, ¹⁻⁸ actuators, ⁹⁻¹¹ fuel cell membranes, ¹²⁻¹⁷ and electrode coatings. ¹⁸⁻²³ Specifically, the growing need to develop safe electrolytes compatible with lithium anodes for electric vehicles further stimulates research in lithium single-ion conducting ionomers, which have lithium cations as the sole mobile counterions. ²⁴⁻³¹ While many potential applications require maximizing ion transport and/or dielectric response, most single-ion conducting ionomers exhibit low conductivity and dielectric constant. ^{2, 32-41} With mobile counterions, the dielectric response for ion-containing polymers strongly correlates with the charge transport. ^{32, 33, 36, 37, 40, 42-47} Understanding the

correlation between dielectric response and charge transport offers new perspectives to optimize energy materials design. For example, raising the dielectric constant has shown the potential to promote ion transport.^{11, 47-54}

Lithium single-ion conducting ionomers based on poly(ethylene oxide) (PEO) and polymer-fixed sulfonylimide counterions exhibit the highest conductivities among different polymerized anions and have demonstrated success in battery testing. 4, 24, 29, 55-65 Recently, it has been shown that the superior conductivity for these sulfonylimide-lithium ionomers compared with sulfonate-lithium ionomers is due to the more weakly aggregated morphology of the former. 66 In particular, high-ion-content sulfonylimide-lithium ionomer exhibits an extremely high dielectric constant (> 100 at 120 °C), which increases with temperature. This behavior differs from typical dipolar relaxation, for which the thermal randomization of dipoles reduces the dielectric constant at higher temperature. 97-69 Understanding such distinctive relaxation phenomena and their relevance to charge transport can impact the design and implementation of electrolytes in many applications where dielectric and transport properties are of primary interest.

Here, we re-analyzed the experimental data for a series of PEO-based sulfonylimide-lithium single-ion conducting ionomers (which we call "MTLi" – see **Figure 1**) from a prior study. ⁶⁶ To further understand the unique dielectric response and ion conduction behavior of MTLi, we employed DFT computation with a simple four-state model which is used to represent the many ionic states present in ionomers. The relative populations of the four states (contact ion pair, quadrupole, triple cation, and triple anion) are assessed based on a cluster-continuum solvation model, which takes the specific interactions between Li⁺ and the ether oxygen lone pairs of PEO

into account by including explicit dimethyl ether molecules.⁷⁰ The calculation results suggest significant amounts of Li⁺ in all the ionic states, in contrast to the dominant presence of the quadrupole state previously discussed for sulfonate-lithium ionomers,^{33, 35, 36, 66, 71} that suggests strong ion aggregation. Our DFT results agree with an MD simulation for PEO-based sulfonylimide-lithium single-ion conducting ionomers, where an easy reorganization of ion aggregates was reported.⁷² The combination of experimental and simulation results implies that Li⁺ can hop along the ion aggregates with small ion aggregation spacing and low cluster dissociation energy between the neutral and charged states. Such mechanism rationalizes the extremely high dielectric constant and low Haven ratio which will be further discussed in this study. Therefore, the high dielectric constant is a consequence rather than the cause of the ion transport for high ion content PEO-based sulfonylimide-lithium ionomers.^{40, 42, 43}

This manuscript is organized as follows: we first discuss the four-state model based on a cluster-continuum DFT computation. The implications of the calculated results are further illustrated based on the experimental data from X-ray, dielectric relaxation spectroscopy (DRS) and pulsed field gradient nuclear magnetic resonance (PFG-NMR). X-ray scattering at 393 K, dielectric relaxation spectroscopy (DRS) measured with a sample thickness of 0.1 mm, and the measured Li diffusion coefficient from pulsed field gradient nuclear magnetic resonance (PFG-NMR) are reproduced from Ref. 66. X-ray scattering at 303 K and DRS spectra measured with larger sample thickness (1.7 mm) for the lowest ion content ionomer are presented in this study. Lastly, the correlation between ion conduction and dielectric response is discussed. The unique dielectric response and high ion conduction for high ion content MTLi is perhaps attributed to Li⁺ hopping along ion aggregates due to comparably low ion cluster dissociation energy and small spacing

between aggregates (short hopping distance). Although such an ion conduction mechanism cannot be validated experimentally, MD simulations have predicted such a hopping mechanism for some ionomers with weak ionic interactions.^{72, 73} The proposed ion conducting mechanism ties in nicely with our experimental and DFT simulation work, and suggests that delocalized ion chemistries could be the path forward to create soft single-ion conductors with superior ionic conductivity.

Experimental

Synthesis and characterization of the PEO-based sulfonylimide-lithium ionomers MTLi20, MTLi37, and MTLi52 have been reported in our previous study.⁶⁶ Here, we briefly summarize the experimental results for the synthesized MTLi ionomers. The structure of the synthesized MTLi is shown in **Figure 1** with random monomer distribution as previously discussed.⁶⁶ **Table 1** summarizes the main characterization results from our previous study⁶⁶ for MTLi including dispersity \boldsymbol{p} , molecular weight \boldsymbol{M}_n , stoichiometric Li⁺ number density \boldsymbol{n}_0 , glass transition temperature T_g , the static dielectric constant ε_s , and the aggregation number (AN) showing raising ε_s with increased ion content.

Figure 1. Chemical structure of the investigated ionomer MTLi. The "M" in MTLi comes from the *m*ethacrylate monomer containing the counterion, and the "T" comes from the [(*t*rifluoromethane)sulfonamidosulfonyl]propyl counterion moiety.

Table 1. Characterization results of synthesized single-ion conducting ionomers MTLi reproduced from Ref 66.⁶⁶

Sample ^a	$m{ heta}^{ m b}$	$M_{\rm n}{}^{\rm c}$	n ₀	$T_{ m g}{}^{ m d}$	Es	ANe
		g/mol	nm ⁻³	K	(393 K)	
MTLi20	1.33	68970	0.29	223	29	5
MTLi37	1.31	61500	0.58	244	72	9
MTLi52	1.25	63100	0.88	271	132	13

- a. Numbers on the right of the polymer abbreviation indicate the ion content (mol%) in the random copolymer (e.g., the ion content for MTLi20 is 20 mol%).
- b. Measured with SEC in 0.05 M LiBr/DMF based on poly(ethylene glycol) standards.
- c. Based on NMR end-group analysis.
- d. Measured with DSC with a heating and cooling rate of 20 K/min.
- e. Aggregation number calculated from X-ray aggregate spacing.

Dielectric Relaxation Spectroscopy (DRS)

To further understand the dielectric response of MTLi, we measured the dielectric response of MTLi ionomers with different sample thickness. In addition to the standard parallel plate sample cell using the silica spacer with a thickness of 0.1 mm, we performed new measurements using our homebuilt liquid cell with significantly larger thickness (d = 1.7 mm) under the same measurement condition to push the onset of electrode polarization to lower frequency. The new measurement

discussed in this study reveals two separate peaks for MTLi20 which validates the presence of two underlying relaxation processes for MTLi ionomers (**Figure 6a, Figure S1, 2**). Excellent agreement between the liquid and sandwich cells confirms the thickness-independent dielectric response (**Figure S2**) and helps with the spectra fitting to determine the characteristic relaxation time and relaxation strength with suppressed electrode polarization contribution. Fitting details can be found in SI. For MTLi37 and MTLi52, measurements were attempted with d = 1.7 mm and the spectra was shown in **Figure S3**. However, the spectra from d = 1.7 mm for MTLi37 and MTLi52 are not further analyzed due to the difficulties of controlling precise sample thickness with homebuilt liquid cell, and only the spectra from d = 0.1 mm are fitted and further analyzed.

DFT Computations

DFT computations were performed with Gaussian09 software to calculate the energy of different Li⁺ states using a cluster continuum solvation model developed for ionomers.⁷⁰ The computations were performed with DFT B3LYP/6-31G++(d, p) with a PCM solvation model (solvent=diethyl ether). Diethyl ether (DME) represents the ethylene-oxide based polymer matrix well, as validated by previous research,⁷⁰ using the same scale factor of 1.1. DME molecules are explicitly added to the neat Li⁺ and Li⁺ clusters (ion pair TLi, triple cation LiTLi⁺, triple anion TLiT⁻, and quadrupole T₂Li₂) to evaluate the number of DME molecules in the first solvation shell. The computed Li⁺ solvation energy and the number of DME in the first solvation shell agree with the literature value despite a slightly larger basis set.⁷⁰ Optimized cluster geometries from Gaussian calculations are shown in **Figure 2**. Li⁺ associates with four oxygens from either the sulfonylimide anion or the DME molecules in each geometry.

An isolated Li⁺ cation binds with oxygens on four DME molecules. Li⁺ in a contact ion pair (TLi) binds monodentate to one oxygen on the sulfonylimide anion and three DME oxygens. The negative triple ion (TLiT⁻) has Li⁺ binding to single oxygens on two different sulfonylimide anions and two DME oxygens. The positive triple ion (LiTLi⁺) has two Li⁺, each binding to different oxygens on sulfonylimide and three DME oxygens. The quadrupole (T₂Li₂) has two Li⁺, each binding to different oxygens on the two sulfonylimide anions and two DME oxygens.

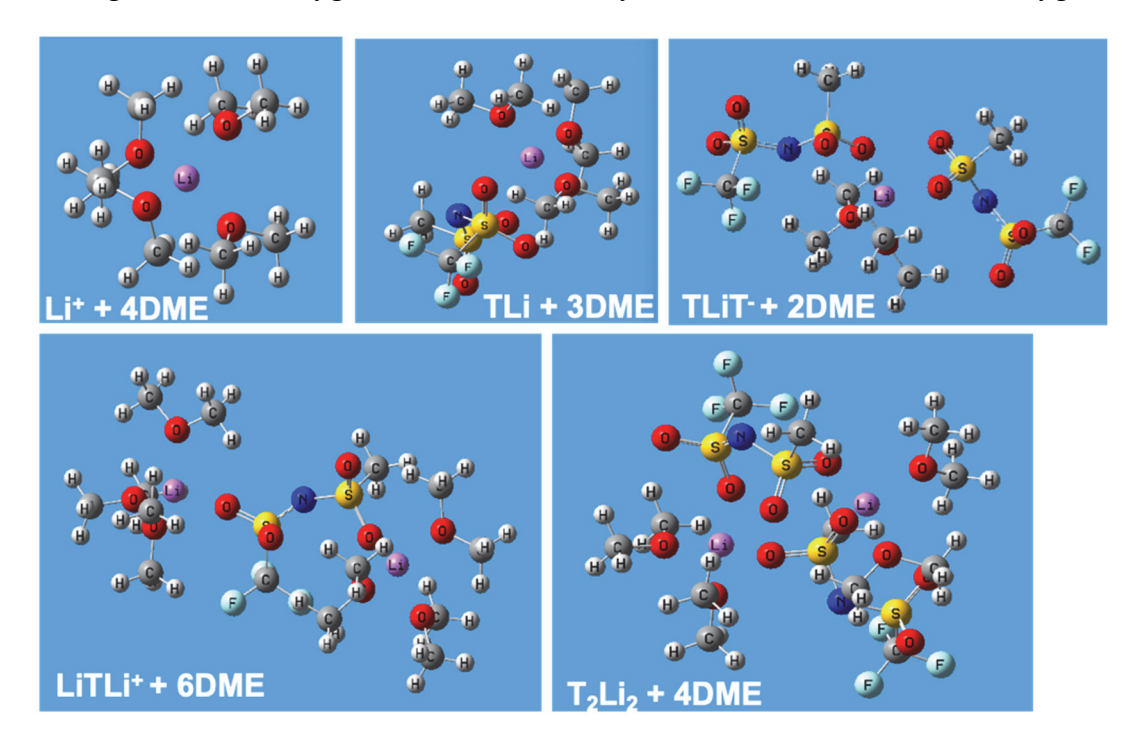


Figure 2. Optimized cluster geometry for Li + 4DME (lone Li⁺ state), TLi + 3DME (ion pair state), TLiT⁻ + 2DME (triple anion state), LiTLi⁺ + 6DME (triple cation state), and T₂Li₂ + 4DME (quadrupole state). Carbon atom (C): dark grey. Hydrogen atom (H): light grey. Oxygen atom (O): red. Sulfur atom (S): yellow. Nitrogen atom (N): blue. Lithium atom (Li): pink. Fluorine atom (F): cyan.

Results and Discussion

To enable further understandings and molecular insights on the dielectric response and ion conduction for the MTLi ionomers based on the experimental results reported in our previous study, 66 DFT computation is employed to calculate the representative ion states based on four-state model which are most relevant to the dielectric response and charge transport. We first illustrate the concept of the four-state model shown in Figure 3a. The four-state model simplifies the complicated ion states present in ionomers to two dissociated states: triple cation LiTLi⁺ and triple anion TLiT and two associated states: ion pair TLi and quadrupole T₂Li₂ (Figure 3a).^{70, 74} The energy of the four ion states are calculated with a cluster-continuum solvation model (CCM) with explicitly added solvent molecules to represent the specific interaction known between Li⁺ and ethers. 70, 75-79 Dimethyl ether (DME) is selected as the solvent, as suggested in a previous study, to represent the neutral PEO matrix. 70 Solvation energy is computed with different number of DME to determine the number of DME within the first solvation shell for the four ion states. The DME solvated neat Li⁺ state is also included for comparison. Figure 3b plots the solvation energy $\Delta E_{solvation}^{CCM}(N)$ as a function of the number of DME molecules for the DME-ion complex cluster as:

$$\Delta E_{solvation}^{CCM}(N) = -E_{cluster+NDME}^{PCM} + E_{cluster}^{PCM} + NE_{DME}^{PCM}$$
 Eq. 1

The onset of the $\Delta E_{solvation}^{CCM}$ (N) plateau gives the number of DME in the first solvation shell (i.e., adding more DME molecules does not further lower the system energy), which consists of 6 DME molecules for the LiTLi⁺, 4 DME for the T₂Li₂, 3 DME for the TLi, 2 DME for the TLiT⁻ and 4 DME for Li⁺. The 4 DME calculated for Li⁺ agrees with other study despite a slightly larger basis set.⁷⁰ The distance between Li⁺ and the oxygen atom from the DME molecule is 2.0 ± 0.1 Å, which is consistent with similar calculations for Li⁺ and ether-based solvents.^{70, 78, 80-83}

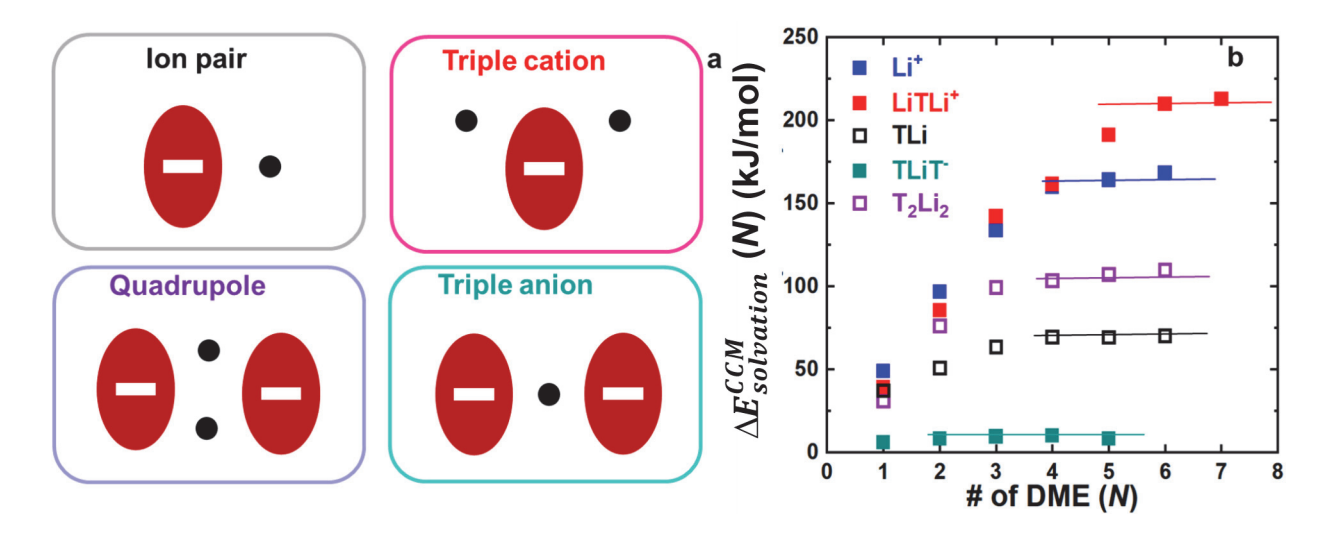


Figure 3. DFT computation based on the four-state model. (a) Illustration of the four-state model. The black circle represents the Li⁺, and the red ellipse represents the sulfonylimide anion. (b) Calculated $\Delta E_{solvation}^{CCM}$ based on Eq. 1 with respect to the number of DME molecules. The solvation of Li⁺ with DME is included for comparison (blue filled squares). Filled red squares represent the LiTLi⁺. Open purple squares represent T₂Li₂. Open black squares represent the TLi. Filled cyan squares represent TLiT⁻.

The interaction energy per mole of Li⁺ for each DME-solvated ion state (ion pair, triple cation, triple anion, quadrupole, and neat Li⁺) $\Delta E_{interaction}^{CCM}$ are computed with respect to the ground state based on neat Li⁺, T⁻ and DME as:

$$\Delta E_{TLi+3DME}^{CCM} = -E_{TLi+3DME}^{PCM} + E_{Li+}^{PCM} + E_{T-}^{PCM} + 3E_{DME}^{PCM}$$
 Eq. 2

$$\Delta E_{LiTLi+6DME}^{CCM} = (-E_{LiTLi+6DME}^{PCM} + 2E_{Li+}^{PCM} + E_{T-}^{PCM} + 6E_{DME}^{PCM})/2$$
 Eq. 3

$$\Delta E_{TLiT+2DME}^{CCM} = -E_{TLiT+2DME}^{PCM} + E_{Li+}^{PCM} + 2E_{T-}^{PCM} + 2E_{DME}^{PCM}$$
 Eq. 4

$$\Delta E_{T2Li2+4DME}^{CCM} = (-E_{T2Li2+4DME}^{PCM} + 2E_{Li+}^{PCM} + 2E_{T-}^{PCM} + 4E_{DME}^{PCM})/2$$
 Eq. 5

$$\Delta E_{Li+4DME}^{CCM} = -E_{Li+4DME}^{PCM} + E_{Li+}^{PCM} + 4E_{DME}^{PCM}$$
 Eq. 6

The computed value based on **Eq. 2–6** is compared in **Figure 4**, showing the interaction energy as follows: $\Delta E_{TLiT+6DME}^{CCM} > \Delta E_{T2Li2+4DME}^{CCM} > \Delta E_{TLi+3DME}^{CCM} > \Delta E_{LiTLi+6DME}^{CCM} > \Delta E_{Li+4DME}^{CCM}$. The quadrupole state is favored over the ion pair state, and the triple cation state is preferable to the DME-solvated Li⁺. The highest ΔE is for the TLiT⁻ negative triple ion because the TLiT⁻ cluster is more stable than the lone anion state.

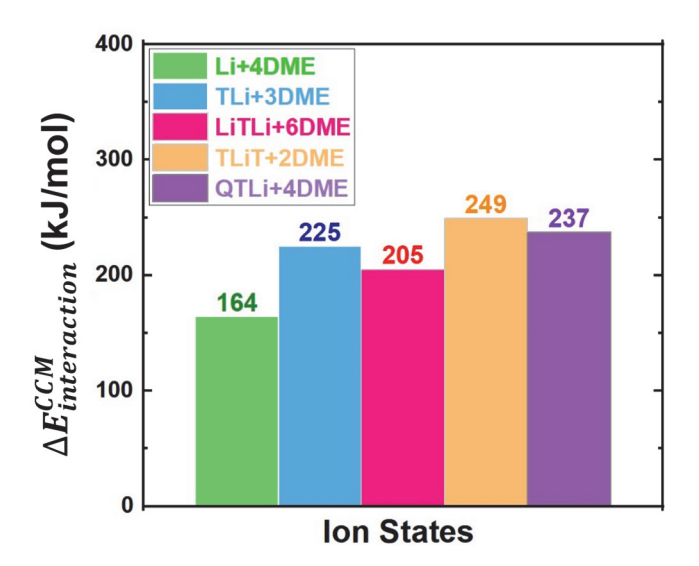


Figure 4. Interaction energy per mol of Li⁺ $\Delta E_{interaction}^{CCM}$ calculated with DFT using cluster solvation model based on **Eq. 2–6**. These $\Delta E_{interaction}^{CCM}$ are the net depth of the attractive well; larger ΔE means a more favored ion state.

In addition to the interaction energy, the energy difference between the associated cluster and the dissociated cluster $\Delta E^{CCM}_{dissociation}$ is calculated, and the results are listed in **Table 2**. Dissociation from quadrupole T₂Li₂ to DME solvated Li⁺ (Li-DME) results in the highest $\Delta E^{CCM}_{dissociation}$. Ion pair TLi dissociating into triple cation LiTLi⁺ and triple anion TLiT⁻ gives the lowest $\Delta E^{CCM}_{dissociation}$. The trend of $\Delta E^{CCM}_{dissociation}$ implies that: 1) significant aggregation with large aggregation number is not favorable; 2) the possibility of Li⁺ to occupy both charged and neutral states; and 3) solvated

 ${\rm Li^+}$ is not the main contributor to ion conduction. The highest $\Delta E^{CCM}_{dissociation}$ to form single ${\rm Li^+}$ solvated by 4 DME (Li-DME) agrees with a recent MD simulation result which suggests that ${\rm Li^+}$ transport through clusters is more favorable than through the PEO matrix.⁷²

Table 2. Energy difference between associated and dissociated clusters per mol Li⁺.

Associated →	Energy of	Energy of	$\Delta E_{dissociation}^{CCM}$	
dissociated	Associated states	Dissociated states	(kJ/mol)	
$T_2Li_2 \rightarrow 2TLi$	E(T ₂ Li ₂ +4DME) +	2*E(TLi+3DME)	12.8	
	2*E(DME)			
$T_2Li_2+TLi \rightarrow$	$E(T_2Li_2+4DME) +$	E(TLiT ⁻ +2DME) +	12.9	
LiTLi ⁺ +TLiT ⁻	E(TLi+3DME) + E(DME)	E(LiTLi ⁺ +6DME)		
$T_2Li_2 \rightarrow TLiT$	$E(T_2Li_2+4DME)$	$E(Li^++4DME) +$	32.3	
+(Li-DME) ⁺		E(TLiT ⁻ +2DME)		
3TLi→	3*E(TLi+3DME)	E(TLiT ⁻ +2DME) +	5.0	
LiTLi ⁺ +TLiT ⁻		$E(LiTLi^++6DME) + E(DME)$		

a. $\Delta E_{dissociation}^{CCM}$ = (Energy of the dissociated states – Energy of the associated states)/mol of Li⁺.

DFT computations suggest that Li⁺ can be found in all the states due to the similar interaction energy for different ion states (**Figure 4**) and moderate dissociation energy between associated and dissociated clusters (**Table 2**). The interaction energy and dissociation energy without explicitly added DME are summarized in **Figure S4** and **Table S3**, which highlights the solvation effect of DME in lowering the dissociation energy and the interaction energy for charged ion states

(i.e., LiTLi⁺ and (Li-DME)⁺). The solvation effect arises from the comparable electronegativity of an oxygen atom from DME (-0.39 e) versus an oxygen atom of a sulfonylimide anion (-0.56 e) when each are bound to Li⁺ (**Figure 2**).

Different ion states contribute differently to the dielectric response and the ion conduction. The ion pair TLi contributes to the dielectric response and the measured D_{Li^+} since TLi can move with the segmental motion of the polymer but not to ionic conductivity since the pair is net neutral. The quadrupole T₂Li₂ represents the simplest ion aggregate and in some sense all ion aggregates composed of multiple ion pairs which barely contribute to dielectric response and the measured Li⁺ diffusion, since such aggregates cannot move. The positive triple ion state LiTLi⁺ significantly contributes to the measured D_{Li^+} and conductivity σ_{DC} , since this state has a positive charge and can move by polymer segmental motion. The negative triple ion TLiT stabilizes the anions (since the PEO matrix barely solvates the anions) and does not contribute to either dielectric constant or ionic conductivity, since TLiT cannot move. The presence of such negatively charged clusters has been reported for PEO/LiTFSI electrolytes.^{84, 85} Based on the different ion states calculated with DFT, experimental data from X-ray scattering, dielectric relaxation spectroscopy and PFG-NMR will be further discussed, suggesting that the high ion content MTLi (i.e., MTLi52) demonstrates a novel ion hopping mechanism which results in significant dielectric response and promoted ion conduction at elevated temperatures. 72, 73

The first piece of experimental data is from X-ray scattering, which indicates a weakly aggregated morphology with small spacing between aggregates.⁶⁶ **Figure 5** compares the scattering pattern for MTLi at ambient (303 K) and at elevated temperature (393 K, reproduced from Ref 66).⁶⁶ As

discussed in Ref 66,⁶⁶ three characteristic peaks are identified: a low-q peak at 2.5 nm⁻¹ attributed to the spacing between ion aggregates ($q_{aggregates}$), a secondary high-q peak at 9.0 nm⁻¹ attributed to the spacing between solvated ions mostly from anion-anion correlation due to its higher electron density contrast (q_{anion}), and a high-q peak at 10.5 nm⁻¹ attributed to the amorphous halo dominated by the scattering of pendant PEO9 chains and neighboring ions ($q_{amorphous}$).^{34, 35, 41, 86, 87} Raising temperature drives the formation of ion aggregates indicated from the increased relative intensity ($I(q)_{aggregate}$ / $I(q)_{amorphous}$) at 393K than 303 K. Temperature has negligible impact on the location of the peak positions for $q_{aggregates}$, suggesting that the corresponding spacing is independent of temperature. The spacing between ion aggregates for MTLi is smaller than typical ionomers with harder anions such as sulfonate.^{34, 35, 41} The smaller spacing indicates a lower average aggregation number (AN, the average number of Li⁺ per cluster, see **Table 1**) which can facilitate Li⁺ hopping along the aggregates as implied from a recent MD study for PEO-based ionomers.⁷²

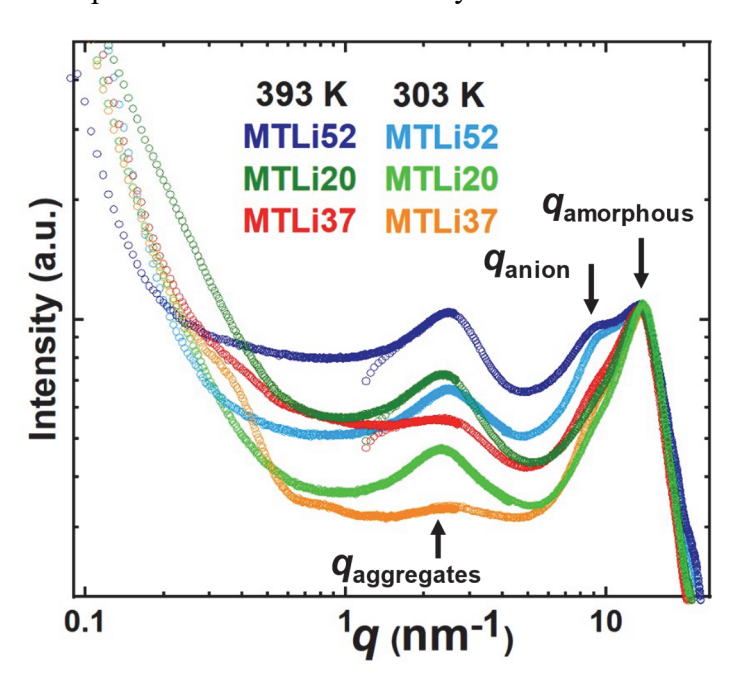


Figure 5. X-ray scattering patterns of MTLi52, MTLi37, and MTLi20 at 393 K and 303K. Each pattern is shifted vertically on the logarithmic intensity scale to superimpose the peaks of the

amorphous halos (the highest q peaks). Data at 393 K is reproduced from Figure 3a of J. *Mater*. *Chem. C*, 2022, 10, 14569. Copyright 2022 The Royal Society of Chemistry.

Ion states also impact the dielectric and conductivity spectra from DRS, which further supports the ion hopping mechanism. Noticeably, MTLi52 shows significant relaxation strength which increases with raising temperature despite its most aggregated morphology (**Figure 5**). Rather than showing one broad relaxation peak as observed for other PEO-based sulfonate lithium ionomers,^{2, 33, 41, 66} the DRS spectra of MTLi reveals a significant secondary relaxation termed α_2 after the onset of DC conductivity. The presence of two underlying relaxation processes is exemplified with MTLi20 measured with larger sample thickness (d = 1.7 mm) to push the onset of electrode polarization to lower frequency (**Figure 6a, Figure S2a**). Consistent results are obtained with different sample thickness which help resolve the secondary α_2 from the high frequency α process (**Figure S1**). For MTLi37 and MTLi52, only one broader peak was resolved with d = 1.7 mm (**Figure S3**) therefore only the spectra measured from samples with d = 0.1 mm were further analyzed due to the difficulties of controlling sample thickness for high T_g samples.

Characteristic relaxation frequency and relaxation strength can be obtained from fitting dielectric spectra shown in **Figure 6a** and **Figure S1**. **Figure 6a** reveals a strong correlation between ion transport and dielectric response. Real permittivity ε' (open pink circles), imaginary permittivity ε'' (open gray circles), and the derivative formula of real permittivity $\varepsilon_{\rm der}(\omega) = -\frac{\pi}{2} \frac{\partial \varepsilon'(\omega)}{\partial \ln \omega}$ (open green circles) were plotted with fitting details included in Supporting Information (**Figure S1** and **Table S1**). In addition to the dielectric spectra, conductivity spectra are plotted as the real conductivity σ' (open blue squares) and the imaginary conductivity σ'' (open purple squares). The

characteristic frequencies for the α and α_2 processes ω_α and $\omega_{\alpha 2}$ from dielectric spectra are marked with vertical lines (solid blue line and dashed red line). Two dielectric constants are determined: the static dielectric constant ε_s indicated with red solid line and the Coulombic dielectric constant ε_c indicated with blue solid line. At low frequencies, the electrode polarization dominates the spectra, and the peak for ε " indicates the characteristic frequency for electrode polarization (EP, ω_{EP}) which depends on sample thickness (**Figure S2a**). The ω_{EP} and ω_α can also be determined from conductivity spectra: the low-frequency peak due to EP can be found from the σ " spectra. At high frequency, the ω_α approximates the frequency of the onset of DC conductivity from the σ ' spectra (ω_σ). Between ω_{EP} and ω_α is the $\omega_{\alpha 2}$, suggesting that α_2 occurs after the onset of DC conductivity which will be further discussed for its relevance with different ion states.

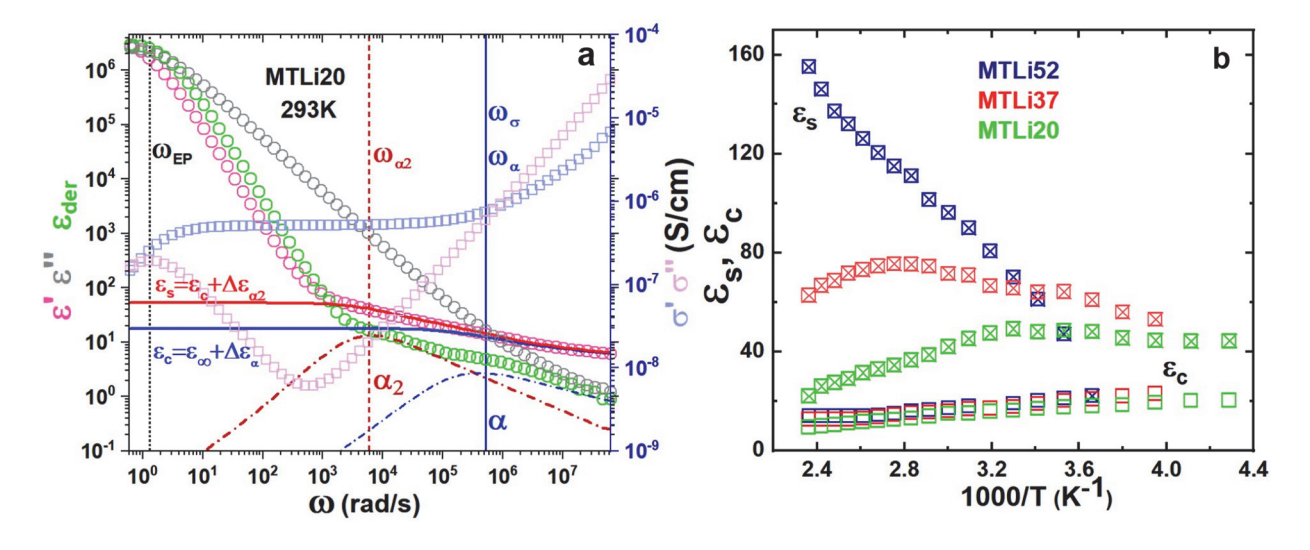


Figure 6. DRS spectra and the determination of ε_s and ε_c . (a) Dielectric spectra for MTLi20 at 293 K with d = 1.7 mm. (b) Temperature dependence of static dielectric constant ε_s (crossed symbols, reproduced from Figure 4c of J. *Mater. Chem. C*, 2022, 10, 14569. Copyright 2022 The Royal Society of Chemistry)⁶⁶ and Coulombic dielectric constant ε_c (open symbols, this study). The Coulombic dielectric constants are typical of all PEO-based ionomers while the static dielectric constant of MTLi52 is surprisingly large at high temperatures.

Temperature dependence of low-frequency ε_s and high-frequency ε_c are compared in **Figure 6b** with the ε_s data reproduced from Ref 66.66 Noticeable, the high temperature ε_s increases with raising ion content, and the ε_s of MTLi52 reaches ~160 at 150 °C. Such high ε_s despite more severe ion aggregation (Figure 5) can be understood from the cluster continuum DFT computation which shows low cluster dissociation energy (**Table 2**). The α₂ process is attributed to the Li⁺ exchange and potential cluster reorganization during the charge transport which creates charge separation and results in significant dielectric strength that are much larger than the relaxation strength expected from dipolar relaxation of EO and contact ion pairs. Our DFT computation results align with a recent MD simulation study demonstrating facile reorganization of ion clusters for high ion content PEO-based sulfonylimide lithium ionomer at elevated temperature.⁷² Because the ion exchange and possible cluster reorganization are thermally activated and depend on the ion number density, high ion content MTLi52 demonstrates the highest ε_s at 150 °C. In contrast, ε_c show typical temperature dependence for dipolar relaxation with a moderate value between 10-20.69, 88 The high frequency α is attributed to the rotation of polar ethylene oxide groups as reported for other PEO-based lithium ionomers which precedes diffusive ion motion. 32, 33, 40, 43, 48

Ion states also impact the measured PFG-NMR results which depend on how Li⁺ sample different ion states at the measurement temperatures. **Figure 7a** compares σ_{DC} (open squares) and σ_{NMR} (filled stars) from the D_{Li^+} reported in Ref 66.⁶⁶ Despite the lowest σ_{DC} for MTLi52 at ambient temperature, its σ_{DC} emulates that of MTLi20 and MTLi37 at 423 K. σ_{NMR} for MTLi52 agrees well with σ_{DC} , while σ_{NMR} is higher than σ_{DC} for MTLi20 and MTLi37. The ratio of σ_{NMR} and σ_{DC} gives the Haven ratio H ($H = \sigma_{NMR} / \sigma_{DC}$). The value of H depends on the ion-ion correlation for the

system of interests, with H = 1 implying fully independent ion motions (as in dilute solution). ⁸⁹⁻⁹² In single-ion conducting ionomers, one main contributor to the higher H is the formation of ion pairs (cation-anion correlation) since the diffusivity of the polymerized ions is much lower than the mobile counterion. $^{71, 93, 94}$ The temperature dependence of Haven ratio H is shown in Figure 7b, reproduced from Ref 66.66 Ion hopping explains the remarkably low H (~1) observed for MTLi52 in the 373-423 K range (below which the D_{Li^+} cannot be measured due to fast spin relaxation) which indicates that during random motions (diffusion) the majority of Li⁺ in MTLi52 is in a state with a net charge, as opposed to some ions undergoing ion pair motion.^{71, 93, 94} In contrast, higher H for lower ion content MTLi20 and MTLi37 implies the pairwise diffusion of Li⁺ that contributes to D_{Li^+} but not σ_{DC} (hence higher σ_{NMR} than σ_{DC} and thus higher H).^{71, 93, 94} Although ion aggregation reduces the D_{Li+} for MTLi52 compared with MTLi20 and MTLi37,⁶⁶ it also reduces the negative anion contribution to the measured σ_{DC} . Because of the small aggregateaggregate spacing ($d_{\text{aggregates}} = 2\pi/q_{\text{aggregates}}$, Figure 5) and low dissociation energy (Table 2), Li⁺ is able to hop among the aggregates for the most aggregated MTLi52 at elevated temperature, resulting in lower H (~ 1) and comparable σ_{DC} to the lower ion content MTLi20 and MTLi37.^{71,93} This scenario is very different from high ion-content PEO-based ionomers with more charge localized anions (e.g., sulfonate), where raising ion content results in much worse σ_{DC} and higher H since those ionomers form discrete aggregates with larger spacing and drastically increased aggregation number.^{2, 33, 41, 66}

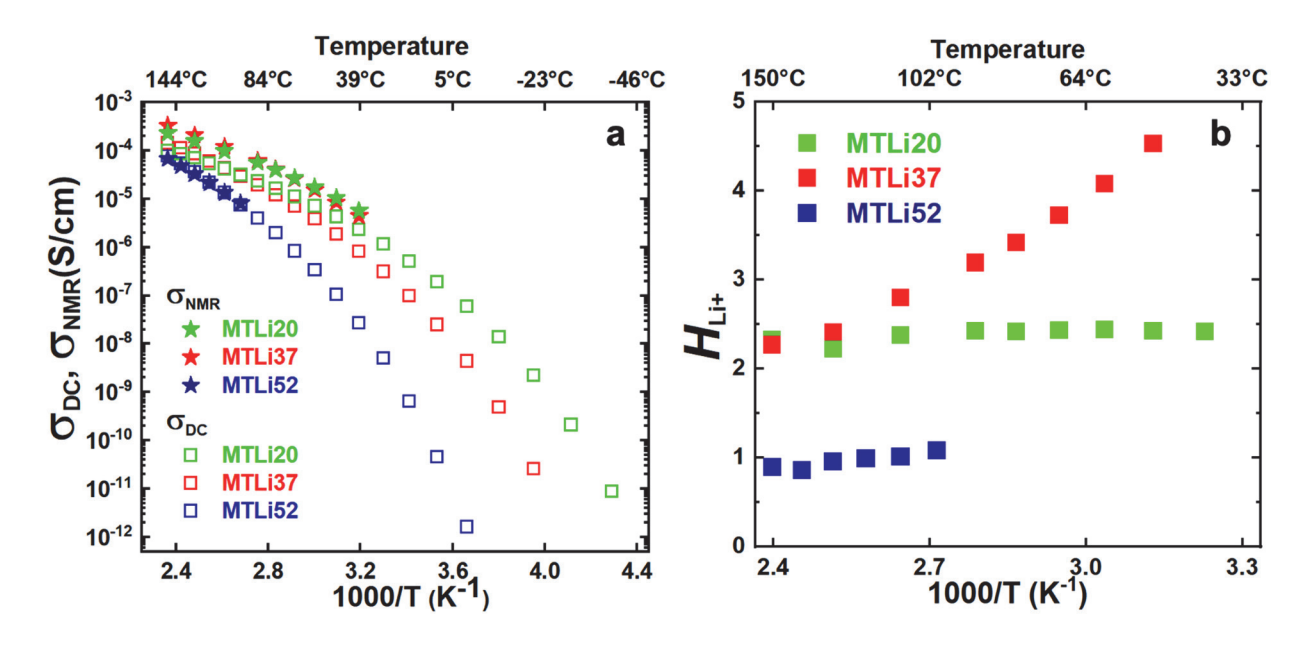


Figure 7. (a) DC conductivity σ_{DC} measured with DRS (open symbols, reproduced from Figure 2a of J. *Mater. Chem. C*, 2022, 10, 14569. Copyright 2022 The Royal Society of Chemistry) and NMR conductivity σ_{NMR} (stars) based on $\sigma_{NMR} = n_0 e^2 \frac{D_{Li+,PFG}}{kT}$ (n_0 is the stoichiometric Li⁺ number density listed in **Table 1**). (b) Temperature dependence of Haven ratio $H = \sigma_{NMR} / \sigma_{DC}$ reproduced from Figure 6a of J. *Mater. Chem. C*, 2022, 10, 14569. Copyright 2022 The Royal Society of Chemistry. ⁶⁶ The surprising result is that Haven ratio is unity for MTLi52, which suggests that ion motion is dominated by ion states with a net charge (not ion pairs).

The molecular scenario of different ion states for MTLi calculated with DFT ties in nicely with the experimental data from X-ray, DRS and PFG-NMR where MTLi52 demonstrates high dielectric constant (> 150 at 150 °C), low Haven ratio ($H \sim 1$), and comparable σ_{DC} despite stronger ion aggregation than lower ion content MTLi20 and MTLi37. Furthermore, the correlation between ion conduction and dielectric response can be understood based on the contributing ion states. **Figure 8a** demonstrates the temperature dependence of ω_{α} (open symbols), $\omega_{\alpha 2}$ (crossed symbols), and ω_{EP} (filled symbols) compared with the measured D_{Li+} (stars) from PFG-NMR.⁶⁶

The D_{Li^+} is vertically shifted and can be superimposed nicely with the ω_{α} , indicating the diffusion length scale is roughly independent of temperature. The similar temperature dependence between the ω determined from DRS and the D_{Li^+} (stars) from PFG-NMR indicates that the origin for the charge transport and dielectric response is similar for ion-containing ionomers, and is relevant to the different ion states Li^+ can sample.

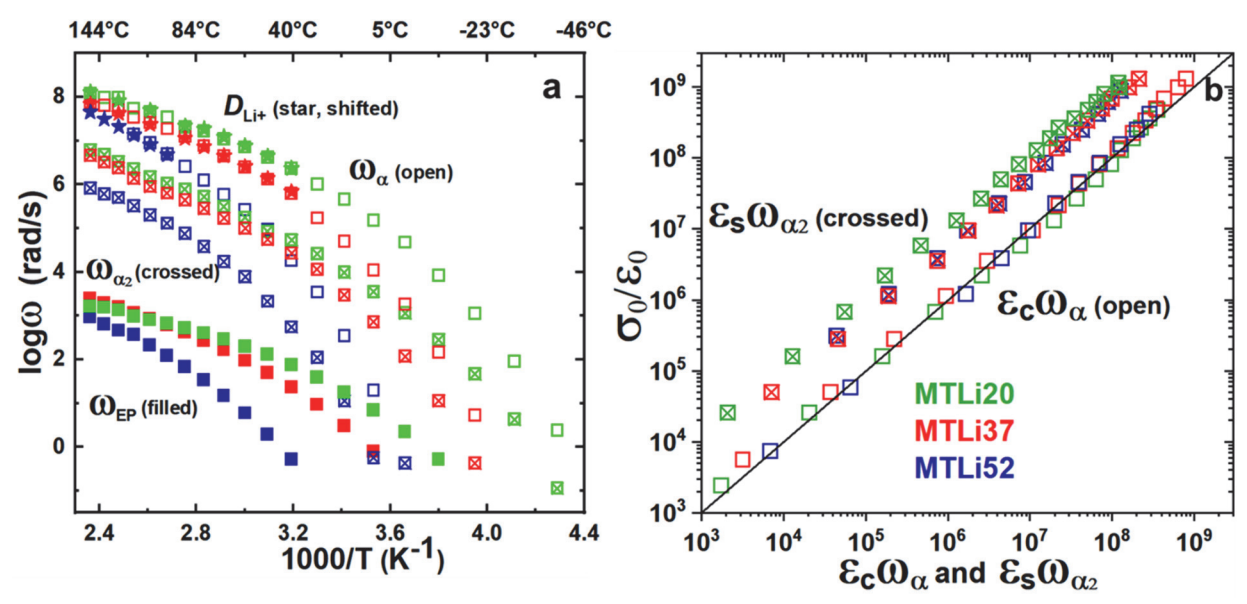


Figure 8. Correlating charge transport to dielectric response. (a) Temperature dependence of ω_{α} (open symbols), $\omega_{\alpha 2}$ (crossed symbols), and ω_{EP} (filled symbols from samples with d = 0.1 mm) compared with the measured $D_{Li^{+}}$ (stars) from PFG-NMR. Data for $D_{Li^{+}}$ is reproduced from Figure 2b of J. *Mater. Chem. C*, 2022, 10, 14569. Copyright 2022 The Royal Society of Chemistry.⁶⁶ (b) BNN relationship plotted based on the product of the low-frequency permittivity ε_{s} and the ion rearrangement frequency $\omega_{\alpha 2}$ (crossed symbols) and the product of the Columbic permittivity ε_{c} between the α and α_{2} processes and the ω_{α} (open symbols).

Figure 8b demonstrates the Barton–Nakajima–Namikawa (BNN) relationship. Crossed symbols represent the BNN relationship with the low-frequency $\omega_{\alpha 2}$ (see **Figure 6a** and **Figure 8a**) and the low-frequency "static" dielectric constant ε_s (see **Figure 6**) as:⁹⁵⁻⁹⁷

$$\sigma_{DC} = B\varepsilon_s\varepsilon_0\omega_{\alpha 2}$$
 Eq. 7

Such a BNN relation was empirically proposed long ago and is now understood in terms of ions moving a distance of order the Debye length on the time scale $1/\omega_{\alpha 2}$.⁴⁰ A wide range of *B* (from 0.4–50) was reported for ionomers using the low-frequency ε_s and $\omega_{\alpha 2}$.⁴⁰ Here, the prefactor *B* for MTLi ionomers is 11 for MTLi20, 5 for MTLi37, and 5.5 for MTLi52 (crossed symbols). As previously discussed, the α_2 process involves the contribution from different ion states exchanging during charge transport. Consequently, how the conducting Li⁺ cations sample various ion states could impact the prefactor *B*, resulting in a nonuniform value for ionomers with different chemical compositions.^{40, 42, 43, 52, 98}

Another way to plot the BNN relationship is to use high frequency Coulombic dielectric constant ε_c determined before the onset of diffusive ion motion and the high frequency ω_α (see **Figure 6a**) as:

$$\sigma_{DC} = B\varepsilon_{c}\varepsilon_{0}\omega_{\alpha}$$
 Eq. 8

Scaling with ε_c and ω_a shows nicely superimposed data with B equal to 1 (B = 1 is indicated by the straight line), which is similar to the original BNN scaling observed for ion-conducting inorganic glasses using the onset frequency of DC conductivity ω_{σ} and the corresponding permittivity value $\varepsilon'(\omega_{\sigma})$. ^{99, 100}

The exact slope of 1 for the BNN scaling means that charge transport and dielectric response are coupled, though the magnitude of prefactor B depends on which dielectric constant is used. $^{40, 42, 46, 52,94, 101}$ The same prefactor B obtained for MTLi with different ion contents based on high-frequency ε_c is a consequence of its relevance on the time scale that ions start to exchange states. Therefore, ε_c better represents the polarity of the polymer matrix based on this study and others. $^{40, 42, 43}$ In contrast, the low-frequency ε_s involves significant contribution from the low-frequency α_2 process (the ionic relaxation). The high ε_s measured for MTLi52 at elevated temperature is the consequence rather than the cause of promoted ion transport.

Different ion states impact the dielectric response and charge transport for single-ion conducting ionomers. With low cluster dissociation energy, Li⁺ in MTLi is able to hop along the ion aggregates resulting in the unique dielectric and ion conduction behavior drastically different from typical single-ion conducting ionomers with charge localized polymerized anion.^{2, 33, 41, 66} Rather than relying on the solvated ions for ion conduction, Li⁺ in MTLi is able to hop along the aggregates and contributes to the measured σ_{DC} . Consequently, high ion content MTLi (i.e., MTLi52) exhibits higher ε_s , comparable σ_{DC} and reduced H at elevated temperatures compared with its low ion content counterparts (i.e., MTLi20 and MTLi37) despite a lower $D_{\text{Li+}}$ due to raised T_g and stronger ion aggregation. The unique ion conduction and dielectric behavior for MTLi compared with other lithium ionomers with charge localized polymerized anions highlights the significant impacts of ion states, and implicates the possibility of tailoring the chemistry of ions and polymer matrix to promote dielectric response and ion conduction to overcome the T_g limitation of single-ion conducting ionomers.^{2, 33, 41, 66}

Conclusion

Based on the experimental results for a series of PEO-based sulfonylimide lithium ionomers previously reported, 66 this study uses a cluster continuum DFT computation with explicit solvation of Li⁺ with dimethyl ether molecules representing PEO, to enable a molecular-level understanding for seemingly contradicting experimental results. The complicated ion states are simplified with a four-state model including ion pair, quadrupole, triple cation, and triple anion, which represent the most relevant ion states impacting ion conduction and dielectric response, since all states with two or more anions are effectively crosslinks that cannot move in that state. This DFT computation indicates a low cluster dissociation energy and the possibility of Li⁺ sampling all four different ion states. Consequently, high ion content ionomer MTLi52 exhibits a different ion conduction mechanism at elevated temperature where Li⁺ can hop along clusters, resulting in high ε_s , low H (~1) and comparable σ_{DC} than its lower content counterparts (i.e., MTLi20 and MTLi37) despite a more aggregated morphology. The proposed ion conduction mechanism ties in nicely with the experimental results and is supported by a recent MD simulation. 72

The implication of this study is two-fold. Firstly, it reveals a strong correlation between dielectric response and charge transport; both are impacted by the different ion states the conducting Li⁺ can sample. The high ε_s exemplified by MTLi52 is mainly contributed by the ionic α_2 relaxation, thus the low-frequency ε_s is a *consequence* rather than the cause of charge transport, and is not the effective dielectric constant that controls all reorientational and translational ion motions (that is the Coulombic dielectric constant ε_c which is relevant on the time scale that ions exchange states). Secondly, the fundamental understandings for ion conduction and dielectric response discussed in this study for sulfonylimide lithium ionomers explains why sulfonylimide seems to be one of the

most effective anions found thus far and has shown promising results from battery tests. ^{28, 55}

Charge-delocalized anions are actively being pursued to further promote ionic conductivity for

polymer electrolytes and could overcome the limitation for lithium-conducting ionomers based on

polymer $T_{\rm g}$, ^{28, 60, 66,} including new ones. ^{102, 103}

ASSOCIATED CONTENT

Supporting Information includes I. DRS Analysis of MTLi Ionomers, II. DFT Calculation based

on Cluster Continuum Solvation Model.

The Supporting Information is available free of charge *via* the Internet.

AUTHOR INFORMATION

Corresponding Authors

*E-mail: rhc5@psu.edu and rjh64@psu.edu

ORCID

Wenwen Mei: 0000-0001-9777-3154

Deyang Yu: 0000-0003-0587-1211

Louis A. Madsen: 0000-0003-4588-5183

Ralph H. Colby: 0000-0002-5492-6189

Robert J. Hickey: 0000-0001-6808-7411

Notes

The authors declare no competing financial interest.

24

ACKNOWLEDGMENTS

We thank the National Science Foundation (NSF) for supporting this research through DMR projects 1807934 and 1810194. X-ray scattering measurements were conducted at the 11-BM CMS beamline of the National Synchrotron Light Source II at Brookhaven National Laboratory under proposal no. 306118. Experimental data from X-ray, DRS and PFG-NMR are reproduced from Ref. 66 with permission from the Royal Society of Chemistry.

References

- 1. Sun, X.-G.; Hou, J.; Kerr, J. B. Comb-shaped single ion conductors based on polyacrylate ethers and lithium alkyl sulfonate. *Electrochim. Acta* **2005**, 50, 1139-1147
- 2. Dou, S.; Zhang, S.; Klein, R. J.; Runt, J.; Colby, R. H. Synthesis and Characterization of Poly(Ethylene Glycol)-Based Single-Ion Conductors. *Chem. Mater.* **2006**, 18, 4288-4295
- 3. Allcock, H. R.; Welna, D. T.; Maher, A. E. Single ion conductors—polyphosphazenes with sulfonimide functional groups. *Solid State Ionics* **2006**, 177, 741-747
- 4. Meziane, R.; Bonnet, J. P.; Courty, M.; Djellab, K.; Armand, M. Single-Ion Polymer Electrolytes Based on a Delocalized Polyanion for Lithium Batteries. Electrochim. *Electrochim. Acta* **2011,** 57, 14
- 5. Bouchet, R.; Maria, S.; Meziane, R.; Aboulaich, A.; Lienafa, L.; Bonnet, J.-P.; Phan, T. N. T.; Bertin, D.; Gigmes, D.; Devaux, D.; Denoyel, R.; Armand, M. Single-ion BAB triblock copolymers as highly efficient electrolytes for lithium-metal batteries. *Nat. Mater.* **2013**, 12, 452-457
- 6. Jr., D. T. H.; Balsara, N. P. Polymer Electrolytes. *Annu. Rev. Mater. Res.* **2013**, 43, 503-525
- 7. Ma, Q.; Zhang, H.; Zhou, C.; Zheng, L.; Cheng, P.; Nie, J.; Feng, W.; Hu, Y.-S.; Li, H.; Huang, X.; Chen, L.; Armand, M.; Zhou, Z. Single Lithium-Ion Conducting Polymer Electrolytes Based on a Super-Delocalized Polyanion. *Angew. Chem. Int. Ed.* **2016**, 55, 2521-2525
- 8. Bocharova, V.; Sokolov, A. P. Perspectives for Polymer Electrolytes: A View from Fundamentals of Ionic Conductivity. *Macromolecules* **2020**,
- 9. Lee, A. A.; Colby, R. H.; Kornyshev, A. A. Electroactuation with single charge carrier ionomers: the roles of electrostatic pressure and steric strain. *Soft Matter* **2013**, 9, 3767-3776
- 10. Romasanta, L. J.; Lopez-Manchado, M. A.; Verdejo, R. Increasing the performance of dielectric elastomer actuators: A review from the materials perspective. *Prog. Polym. Sci.* **2015**, 51, 188-211
- 11. Kim, O.; Kim, H.; Choi, U. H.; Park, M. J. One-volt-driven superfast polymer actuators based on single-ion conductors. *Nat. Commun.* **2016**, 7, 13576

- 12. Karlsson, L. E.; Jannasch, P. Polysulfone ionomers for proton-conducting fuel cell membranes: sulfoalkylated polysulfones. *Journal of Membrane Science* **2004**, 230, 61-70
- 13. Lu, S.; Pan, J.; Huang, A.; Zhuang, L.; Lu, J. Alkaline polymer electrolyte fuel cells completely free from noble metal catalysts. *Proc. Natl. Acad. Sci. U. S. A.* **2008**, 105, 20611
- 14. Wang, Y.; Chen, K. S.; Mishler, J.; Cho, S. C.; Adroher, X. C. A review of polymer electrolyte membrane fuel cells: Technology, applications, and needs on fundamental research. *Appl. Energy* **2011**, 88, 981
- 15. Pan, J.; Chen, C.; Zhuang, L.; Lu, J. Designing Advanced Alkaline Polymer Electrolytes for Fuel Cell Applications. *Acc. Chem. Res.* **2012**, 45, 473
- 16. Chen, N.; Lee, Y. M. Anion exchange polyelectrolytes for membranes and ionomers. *Progress in Polymer Science* **2021**, 113, 101345
- 17. Das, G.; Choi, J.-H.; Nguyen, P. K. T.; Kim, D.-J.; Yoon, Y. S. Anion Exchange Membranes for Fuel Cell Application: A Review. *Polymers* **2022**, 14, 1197
- 18. Stalin, S.; Tikekar, M.; Biswal, P.; Li, G.; Johnson, H. E. N.; Deng, Y.; Zhao, Q.; Vu, D.; Coates, G. W.; Archer, L. A. Designing Polymeric Interphases for Stable Lithium Metal Deposition. *Nano Lett.* **2020**, 20, 5749-5758
- 19. Zheng, G.; Wang, C.; Pei, A.; Lopez, J.; Shi, F.; Chen, Z.; Sendek, A. D.; Lee, H.-W.; Lu, Z.; Schneider, H.; Safont-Sempere, M. M.; Chu, S.; Bao, Z.; Cui, Y. High-Performance Lithium Metal Negative Electrode with a Soft and Flowable Polymer Coating. *ACS Energy Lett.* **2016**, 1, 1247-1255
- 20. Kong, X.; Rudnicki, P. E.; Choudhury, S.; Bao, Z.; Qin, J. Dendrite Suppression by a Polymer Coating: A Coarse-Grained Molecular Study. *Adv. Funct. Mater.* **2020**, 30, 1910138
- 21. Lopez, J.; Mackanic, D. G.; Cui, Y.; Bao, Z. Designing polymers for advanced battery chemistries. *Nat. Rev. Mater.* **2019**, 4, 312-330
- 22. Yu, Z.; Mackanic, D. G.; Michaels, W.; Lee, M.; Pei, A.; Feng, D.; Zhang, Q.; Tsao, Y.; Amanchukwu, C. V.; Yan, X.; Wang, H.; Chen, S.; Liu, K.; Kang, J.; Qin, J.; Cui, Y.; Bao, Z. A Dynamic, Electrolyte-Blocking, and Single-Ion-Conductive Network for Stable Lithium-Metal Anodes. *Joule* **2019**, 3, 2761-2776
- 23. Huang, Z.; Choudhury, S.; Gong, H.; Cui, Y.; Bao, Z. A Cation-Tethered Flowable Polymeric Interface for Enabling Stable Deposition of Metallic Lithium. *J. Am. Chem. Soc.* **2020**, 142, 21393-21403
- 24. Xue, Z.; He, D.; Xie, X. Poly(ethylene oxide)-based electrolytes for lithium-ion batteries. *Journal of Materials Chemistry A* **2015**, 3, 19218-19253
- 25. Wang, Y.; Zhong, W.-H. Development of Electrolytes towards Achieving Safe and High-Performance Energy-Storage Devices: A Review. *ChemElectroChem* **2015**, 2, 22-36
- 26. Varzi, A.; Raccichini, R.; Passerini, S.; Scrosati, B. Challenges and prospects of the role of solid electrolytes in the revitalization of lithium metal batteries. *Journal of Materials Chemistry A* **2016**, 4, 17251-17259
- 27. Zhang, Q.; Liu, K.; Ding, F.; Liu, X. Recent advances in solid polymer electrolytes for lithium batteries. *Nano Research* **2017**, 10, 4139-4174
- 28. Zhou, D.; Shanmukaraj, D.; Tkacheva, A.; Armand, M.; Wang, G. Polymer Electrolytes for Lithium-Based Batteries: Advances and Prospects. *Chem* **2019**, 5, 2326-2352
- 29. Cao, C.; Li, Y.; Feng, Y.; Peng, C.; Li, Z.; Feng, W. A solid-state single-ion polymer electrolyte with ultrahigh ionic conductivity for dendrite-free lithium metal batteries. *Energy Storage Mater.* **2019**, 19, 401-407

- 30. Wang, Q.; Jiang, L.; Yu, Y.; Sun, J. Progress of enhancing the safety of lithium ion battery from the electrolyte aspect. *Nano Energy* **2019**, 55, 93-114
- 31. Zhao, Q.; Stalin, S.; Zhao, C.-Z.; Archer, L. A. Designing solid-state electrolytes for safe, energy-dense batteries. *Nat. Rev. Mater.* **2020**, *5*, 229-252
- 32. Fragiadakis, D.; Dou, S.; Colby, R. H.; Runt, J. Molecular Mobility, Ion Mobility, and Mobile Ion Concentration in Poly(ethylene oxide)-Based Polyurethane Ionomers. *Macromolecules* **2008**, 41, 5723-5728
- 33. Fragiadakis, D.; Dou, S.; Colby, R. H.; Runt, J. Molecular mobility and Li+ conduction in polyester copolymer ionomers based on poly(ethylene oxide). *J. Chem. Phys.* **2009**, 130, 064907
- 34. Wang, W.; Liu, W.; Tudryn, G. J.; Colby, R. H.; Winey, K. I. Multi-Length Scale Morphology of Poly(ethylene oxide)-Based Sulfonate Ionomers with Alkali Cations at Room Temperature. *Macromolecules* **2010**, 43, 4223-4229
- 35. Wang, W.; Tudryn, G. J.; Colby, R. H.; Winey, K. I. Thermally Driven Ionic Aggregation in Poly(ethylene oxide)-Based Sulfonate Ionomers. *J. Am. Chem. Soc.* **2011**, 133, 10826-10831
- 36. Tudryn, G. J.; O'Reilly, M. V.; Dou, S.; King, D. R.; Winey, K. I.; Runt, J.; Colby, R. H. Molecular Mobility and Cation Conduction in Polyether–Ester–Sulfonate Copolymer Ionomers. *Macromolecules* **2012**, 45, 3962-3973
- 37. Liang, S.; Choi, U. H.; Liu, W.; Runt, J.; Colby, R. H. Synthesis and Lithium Ion Conduction of Polysiloxane Single-Ion Conductors Containing Novel Weak-Binding Borates. *Chem. Mater.* **2012**, 24, 2316-2323
- 38. Helen Wang, J. H.; Colby, R. H. Exploring the Role of Ion Solvation in Ethylene Oxide Based Single-Ion Conducting Polyanions and Polycations. *Soft Matter* **2013**, 9, 10275
- 39. Liang, S.; O'Reilly, M. V.; Choi, U. H.; Shiau, H.-S.; Bartels, J.; Chen, Q.; Runt, J.; Winey, K. I.; Colby, R. H. High Ion Content Siloxane Phosphonium Ionomers with Very Low Tg. *Macromolecules* **2014**, 47, 4428-4437
- 40. Choi, U. H.; Ye, Y.; Salas de la Cruz, D.; Liu, W.; Winey, K. I.; Elabd, Y. A.; Runt, J.; Colby, R. H. Dielectric and Viscoelastic Responses of Imidazolium-Based Ionomers with Different Counterions and Side Chain Lengths. *Macromolecules* **2014**, 47, 777
- 41. Wang, J.-H. H.; Yang, C. H.-C.; Masser, H.; Shiau, H.-S.; O'Reilly, M. V.; Winey, K. I.; Runt, J.; Painter, P. C.; Colby, R. H. Ion States and Transport in Styrenesulfonate Methacrylic PEO9 Random Copolymer Ionomers. *Macromolecules* **2015**, 48, 7273-7285
- 42. Choi, U. H.; Lee, M.; Wang, S.; Liu, W.; Winey, K. I.; Gibson, H. W.; Colby, R. H. Ionic Conduction and Dielectric Response of Poly(imidazolium acrylate) Ionomers. *Macromolecules* **2012**, 45, 3974-3985
- 43. Choi, U. H.; Mittal, A.; Price, T. L.; Gibson, H. W.; Runt, J.; Colby, R. H. Polymerized Ionic Liquids with Enhanced Static Dielectric Constants. *Macromolecules* **2013**, 46, 1175-1186
- 44. Choi, U. H.; Liang, S.; O'Reilly, M. V.; Winey, K. I.; Runt, J.; Colby, R. H. Influence of Solvating Plasticizer on Ion Conduction of Polysiloxane Single-Ion Conductors. *Macromolecules* **2014**, 47, 3145-3153
- 45. Liang, S.; Chen, Q.; Choi, U. H.; Bartels, J.; Bao, N.; Runt, J.; Colby, R. H. Plasticizing Li Single-Ion Conductors with Low-Volatility Siloxane Copolymers and Oligomers Containing Ethylene Oxide and Cyclic Carbonates. *J. Mater. Chem. A* **2015**, 3, 21269
- 46. Choi, U. H.; Liang, S.; Chen, Q.; Runt, J.; Colby, R. H. Segmental Dynamics and Dielectric Constant of Polysiloxane Polar Copolymers as Plasticizers for Polymer Electrolytes. *ACS Appl. Mater. Interfaces* **2016**, 8, 3215-3225

- 47. Choi, U. H.; Colby, R. H. The Role of Solvating 12-Crown-4 Plasticizer on Dielectric Constant and Ion Conduction of Poly(ethylene oxide) Single-Ion Conductors. *Macromolecules* **2017**, 50, 5582-5591
- 48. Chen, Q.; Bao, N.; Wang, J.-H. H.; Tunic, T.; Liang, S.; Colby, R. H. Linear Viscoelasticity and Dielectric Spectroscopy of Ionomer/Plasticizer Mixtures: A Transition from Ionomer to Polyelectrolyte. *Macromolecules* **2015**, 48, 8240-8252
- 49. Gavish, N.; Promislow, K. Dependence of the dielectric constant of electrolyte solutions on ionic concentration: A microfield approach. *Phys. Rev. E* **2016**, 94, 012611
- 50. Wheatle, B. K.; Keith, J. R.; Mogurampelly, S.; Lynd, N. A.; Ganesan, V. Influence of Dielectric Constant on Ionic Transport in Polyether-Based Electrolytes. *ACS Macro Lett.* **2017**, 6, 1362-1367
- 51. Wheatle, B. K.; Lynd, N. A.; Ganesan, V. Effect of Polymer Polarity on Ion Transport: A Competition between Ion Aggregation and Polymer Segmental Dynamics. *ACS Macro Lett.* **2018**, 7, 1149-1154
- 52. Choi, U. H.; Price, T. L.; Schoonover, D. V.; Xie, R.; Gibson, H. W.; Colby, R. H. Role of Chain Polarity on Ion and Polymer Dynamics: Molecular Volume-Based Analysis of the Dielectric Constant for Polymerized Norbornene-Based Ionic Liquids. *Macromolecules* **2020**, 53, 10561-10573
- 53. Shen, K. H.; Hall, L. M. Effects of Ion Size and Dielectric Constant on Ion Transport and Transference Number in Polymer Electrolytes. *Macromolecules* **2020**, 53, 10086
- 54. Ma, B.; Olvera de la Cruz, M. A Perspective on the Design of Ion-Containing Polymers for Polymer Electrolyte Applications. *J. Phys. Chem. B* **2021**, 125, 3015-3022
- 55. Bouchet, R.; Maria, S.; Meziane, R.; Aboulaich, A.; Lienafa, L.; Bonnet, J. P.; Phan, T. N. T.; Bertin, D.; Gigmes, D.; Devaux, D.; Denoyel, R.; Armand, M. Single-ion BAB triblock copolymers as highly efficient electrolytes for lithium-metal batteries. *Nat. Mater.* **2013**, 12, 452
- 56. Rolland, J.; Poggi, E.; Vlad, A.; Gohy, J. F. Single-Ion Diblock Copolymers for Solid-State Polymer Electrolytes. *Polymer* **2015**, 68, 344
- 57. Porcarelli, L.; Shaplov, A. S.; Salsamendi, M.; Nair, J. R.; Vygodskii, Y. S.; Mecerreyes, D.; Gerbaldi, C. Single-Ion Block Copoly(ionic liquid)s as Electrolytes for All-Solid State Lithium Batteries. *ACS Appl. Mater. Interfaces* **2016**, 8, 10350
- 58. Porcarelli, L.; Shaplov, A. S.; Bella, F.; Nair, J. R.; Mecerreyes, D.; Gerbaldi, C. Single-Ion Conducting Polymer Electrolytes for Lithium Metal Polymer Batteries That Operate at Ambient Temperature. *ACS Energy Lett.* **2016**, 1, 678
- 59. Porcarelli, L.; Aboudzadeh, M. A.; Rubatat, L.; Nair, J. R.; Shaplov, A. S.; Gerbaldi, C.; Mecerreyes, D. Single-ion triblock copolymer electrolytes based on poly(ethylene oxide) and methacrylic sulfonamide blocks for lithium metal batteries. *J. Power Sources* **2017**, 364, 191-199
- 60. Zhang, H.; Li, C.; Piszcz, M.; Coya, E.; Rojo, T.; Rodriguez-Martinez, L. M.; Armand, M.; Zhou, Z. Single Lithium-Ion Conducting Solid Polymer Electrolytes: Advances and Perspectives. *Chem. Soc. Rev.* **2017**, 46, 797
- 61. Ahmed, F.; Choi, I.; Rahman, M. M.; Jang, H.; Ryu, T.; Yoon, S.; Jin, L.; Jin, Y.; Kim, W. Remarkable Conductivity of a Self-Healing Single-Ion Conducting Polymer Electrolyte, Poly(ethylene-co-acrylic lithium (fluoro sulfonyl)imide), for All-Solid-State Li-Ion Batteries. *ACS Appl. Mater. Interfaces* **2019**, 11, 34930
- 62. Chen, G.; Niu, C.; Chen, Y.; Shang, W.; Qu, Y.; Du, Z.; Zhao, L.; Liao, X.; Du, J.; Chen, Y. A single-ion conducting polymer electrolyte based on poly(lithium 4-styrenesulfonate) for high-performance lithium metal batteries. *Solid State Ionics* **2019**, 341, 115048

- 63. Fdz De Anastro, A.; Porcarelli, L.; Hilder, M.; Berlanga, C.; Galceran, M.; Howlett, P.; Forsyth, M.; Mecerreyes, D. UV-Cross-Linked Ionogels for All-Solid-State Rechargeable Sodium Batteries. *ACS Applied Energy Materials* **2019**, 2, 6960-6966
- 64. Ford, H. O.; Park, B.; Jiang, J.; Seidler, M. E.; Schaefer, J. L. Enhanced Li+ Conduction within Single-Ion Conducting Polymer Gel Electrolytes via Reduced Cation–Polymer Interaction. *ACS Materials Letters* **2020**, *2*, 272-279
- 65. Zhao, Q.; Stalin, S.; Zhao, C. Z.; Archer, L. A. Designing solid-state electrolytes for safe, energy-dense batteries. *Nat. Rev. Mater.* **2020,** 5, 229
- 66. Mei, W.; Yu, D.; George, C.; Madsen, L. A.; Hickey, R.; Colby, R. H. Anion Chemical Composition of Poly(ethylene oxide)-based Sulfonylimide and Sulfonate Lithium Ionomers Controls Ion Aggregation and Conduction. *Journal of Materials Chemistry C* **2022**,
- 67. Debye, P. J. W., *Polar molecules*. Dover publications: 1929.
- 68. Debye, P. Part I. Dielectric constant. Energy absorption in dielectrics with polar molecules. *Trans. Faraday Soc.* **1934**, 30, 679-684
- 69. Onsager, L. Electric Moments of Molecules in Liquids. J. Am. Chem. Soc. 1936, 58, 1486-1493
- 70. Shiau, H.-S.; Liu, W.; Colby, R. H.; Janik, M. J. Cluster-continuum quantum mechanical models to guide the choice of anions for Li+-conducting ionomers. *J. Chem. Phys.* **2013**, 139, 204905
- 71. LaFemina, N. H.; Chen, Q.; Mueller, K. T.; Colby, R. H. Diffusive Flux as a New Metric for Ion-Conducting Soft Materials. *ACS Energy Lett.* **2016**, 1, 1179
- 72. Kadulkar, S.; Brotherton, Z. W.; Lynch, A. L.; Pohlman, G.; Zhang, Z.; Torres, R.; Manthiram, A.; Lynd, N. A.; Truskett, T. M.; Ganesan, V. The Importance of Morphology on Ion Transport in Single-Ion, Comb-Branched Copolymer Electrolytes: Experiments and Simulations. *Macromolecules* **2023**, 56, 2790-2800
- 73. Hall, L. M.; Stevens, M. J.; Frischknecht, A. L. Dynamics of model ionomer melts of various architectures. *Macromolecules* **2012**, 45, 8097
- 74. Liu, W.; Janik, M. J.; Colby, R. H., First Principles Design of Ionomers for Facile Ion Transport. In *Polymers for Energy Storage and Delivery: Polyelectrolytes for Batteries and Fuel Cells*, American Chemical Society: 2012; Vol. 1096, pp 19-44.
- 75. Asai, H.; Fujii, K.; Nishi, K.; Sakai, T.; Ohara, K.; Umebayashi, Y.; Shibayama, M. Solvation Structure of Poly(ethylene glycol) in Ionic Liquids Studied by High-energy X-ray Diffraction and Molecular Dynamics Simulations. *Macromolecules* **2013**, 46, 2369-2375
- 76. Bennington, P.; Deng, C.; Sharon, D.; Webb, M. A.; de Pablo, J. J.; Nealey, P. F.; Patel, S. N. Role of solvation site segmental dynamics on ion transport in ethylene-oxide based side-chain polymer electrolytes. *Journal of Materials Chemistry A* **2021**,
- 77. Blint, R. J. Binding of Ether and Carbonyl Oxygens to Lithium Ion. *J. Electrochem. Soc.* **1995,** 142, 696-702
- 78. Borodin, O.; Smith, G. D. Mechanism of Ion Transport in Amorphous Poly(ethylene oxide)/LiTFSI from Molecular Dynamics Simulations. *Macromolecules* **2006**, 39, 1620
- 79. Deng, C.; Webb, M. A.; Bennington, P.; Sharon, D.; Nealey, P. F.; Patel, S. N.; de Pablo, J. J. Role of Molecular Architecture on Ion Transport in Ethylene oxide-Based Polymer Electrolytes. *Macromolecules* **2021**, 54, 2266-2276
- 80. Eilmes, A.; Munn, R. W. Calculations of the stabilization energies for Li+ ions in poly(ethylene oxide)-based solid electrolytes. *Solid State Ionics* **2005**, 176, 1861-1868

- 81. Baboul, A. G.; Redfern, P. C.; Sutjianto, A.; Curtiss, L. A. Li+–(Diglyme)2 and LiClO4–Diglyme Complexes: Barriers to Lithium Ion Migration. *J. Am. Chem. Soc.* **1999**, 121, 7220-7227
- 82. Jarek, R. L.; Miles, T. D.; Trester, M. L.; Denson, S. C.; Shin, S. K. Solvation of Li+ by Acetone, THF, and Diethyl Ether in the Gas Phase and the Ion–Molecule Association Mechanism. *The Journal of Physical Chemistry A* **2000**, 104, 2230-2237
- 83. Redfern, P. C.; Curtiss, L. A. Quantum chemical studies of Li+ cation binding to polyalkyloxides. *J. Power Sources* **2002**, 110, 401-405
- 84. Pesko, D. M.; Timachova, K.; Bhattacharya, R.; Smith, M. C.; Villaluenga, I.; Newman, J.; Balsara, N. P. Negative Transference Numbers in Poly(ethylene oxide)-Based Electrolytes. *J. Electrochem. Soc.* **2017**, 164, E3569-E3575
- 85. Choo, Y.; Halat, D. M.; Villaluenga, I.; Timachova, K.; Balsara, N. P. Diffusion and migration in polymer electrolytes. *Prog. Polym. Sci.* **2020**, 103, 101220
- 86. Chen, Q.; Liang, S.; Shiau, H.-s.; Colby, R. H. Linear Viscoelastic and Dielectric Properties of Phosphonium Siloxane Ionomers. *ACS Macro Lett.* **2013**, 2, 970-974
- 87. Wang, S.-W.; Liu, W.; Colby, R. H. Counterion Dynamics in Polyurethane-Carboxylate Ionomers with Ionic Liquid Counterions. *Chem. Mater.* **2011**, 23, 1862-1873
- 88. Kremer, F.; Schönhals, A., Broadband Dielectric Spectroscopy. 2002.
- 89. Vargas-Barbosa, N. M.; Roling, B. Dynamic Ion Correlations in Solid and Liquid Electrolytes: How Do They Affect Charge and Mass Transport? *ChemElectroChem* **2020**, 7, 367-385
- 90. Fong, K. D.; Self, J.; McCloskey, B. D.; Persson, K. A. Ion Correlations and Their Impact on Transport in Polymer-Based Electrolytes. *Macromolecules* **2021**, 54, 2575-2591
- 91. Son, C. Y.; Wang, Z.-G. Ion transport in small-molecule and polymer electrolytes. *J. Chem. Phys.* **2020**, 153, 100903
- 92. Popov, I.; Biernacka, K.; Zhu, H.; Nti, F.; Porcarelli, L.; Wang, X.; Khamzin, A.; Gainaru, C.; Forsyth, M.; Sokolov, A. P. Strongly Correlated Ion Dynamics in Plastic Ionic Crystals and Polymerized Ionic Liquids. *J. Phys. Chem. C* **2020**, 124, 17889-17896
- 93. LaFemina, N. H.; Chen, Q.; Colby, R. H.; Mueller, K. T. The diffusion and conduction of lithium in poly(ethylene oxide)-based sulfonate ionomers. *J. Chem. Phys.* **2016**, 145, 114903
- 94. Gainaru, C.; Stacy, E. W.; Bocharova, V.; Gobet, M.; Holt, A. P.; Saito, T.; Greenbaum, S.; Sokolov, A. P. Mechanism of Conductivity Relaxation in Liquid and Polymeric Electrolytes: Direct Link between Conductivity and Diffusivity. *J. Phys. Chem. B* **2016**, 120, 11074
- 95. Namikawa, H. Characterization of the diffusion process in oxide glasses based on the correlation between electric conduction and dielectric relaxation. *J. Non-Cryst. Solids* **1975**, 18, 173-195
- 96. Nakajima, T. 1971 Annual Report, Conference on Electric Insulation and Dielectric Phenomena. **1972**,
- 97. Barton, J. Dielectric relaxation of some ternary alkali-alkaline earth-silicate glasses. *Verres Refract* **1966**, 20, 328-335
- 98. Choi, U. H.; Mittal, A.; Price, T. L.; Lee, M.; Gibson, H. W.; Runt, J.; Colby, R. H. Molecular Volume Effects on the Dynamics of Polymerized Ionic Liquids and their Monomers. *Electrochim. Acta* **2015**, 175, 55-61
- 99. Dyre, J. C. Universal low-temperature ac conductivity of macroscopically disordered nonmetals. *Physical Review B* **1993**, 48, 12511-12526

- 100. Dyre, J. C.; Maass, P.; Roling, B.; Sidebottom, D. L. Fundamental questions relating to ion conduction in disordered solids. *Rep. Prog. Phys.* **2009**, 72, 046501
- 101. Sangoro, J. R.; Iacob, C.; Serghei, A.; Friedrich, C.; Kremer, F. Universal scaling of charge transport in glass-forming ionic liquids. *Phys. Chem. Chem. Phys.* **2009**, 11, 913-916
- 102. Martinez-Ibañez, M.; Sanchez-Diez, E.; Oteo, U.; Gracia, I.; Aldalur, I.; Eitouni, H. B.; Joost, M.; Armand, M.; Zhang, H. Anions with a Dipole: Toward High Transport Numbers in Solid Polymer Electrolytes. *Chem. Mater.* **2022**, 34, 3451-3460
- 103. Qiao, L.; Rodriguez Peña, S.; Martínez-Ibañez, M.; Santiago, A.; Aldalur, I.; Lobato, E.; Sanchez-Diez, E.; Zhang, Y.; Manzano, H.; Zhu, H.; Forsyth, M.; Armand, M.; Carrasco, J.; Zhang, H. Anion π – π Stacking for Improved Lithium Transport in Polymer Electrolytes. *J. Am. Chem. Soc.* **2022**, 144, 9806-9816